atmosphere

MDPI

Article

Comparison of Sensible Heat Fluxes Measured by a Large Aperture Scintillometer and Eddy Covariance System over a Heterogeneous Farmland in East China

Xin Li [1], Zhiqiu Gao [1,2,3,*], Yubin Li [3] and Bing Tong [4]

1 Climate and Weather Disasters Collaborative Innovation Center, Key Laboratory for Aerosol-Cloud-Precipitation of China Meteorological Administration, School of Atmospheric Physics, Nanjing University of Information Science and Technology, Nanjing 210044, China; lixin_91lx@126.com
2 State Key Laboratory of Atmospheric Boundary Layer Physics and Atmospheric Chemistry, Institute of Atmospheric Physics, Chinese Academy of Sciences, Beijing 100029, China
3 School of Geography and Remote Sensing, Nanjing University of Information Science and Technology, Nanjing 210044, China; liyubin@nuist.edu.cn
4 Climate and Weather Disasters Collaborative Innovation Center, Jiangsu Key Laboratory of Agricultural Meteorology, School of Applied Meteorology, Nanjing University of Information Science and Technology, Nanjing 210044, China; tongb1218@163.com
* Correspondence: zgao@mail.iap.ac.cn; Tel.: +86-25-5869-5706

Academic Editor: Gunnar W. Schade
Received: 16 March 2017; Accepted: 31 May 2017; Published: 6 June 2017

Abstract: The sensible heat is an important component in surface energy partitioning over the land surface. This paper compared the sensible heat fluxes measured by a large aperture scintillometer system (LAS) and an eddy covariance system (EC) over a rice paddy with a patch of mulberry seedlings in the east China coastal region during the period from 13 September–11 October 2015. During the observation period, easterlies and northerlies prevailed, and 96% easterlies and northerlies had a speed of 0–6 m s^{-1}. The sensible heat fluxes measured by the two systems reflected that the value of H_{LAS} generally was inclined to be larger than H_{EC} with the average difference of 20.30 W m^{-2}, and the uncertainty for two instruments was less than 17 W m^{-2}. Analysis of the average footprint resulted that the mulberry seedling field always had a higher contribution to LAS than that to EC, which could be the reason that H_{LAS} was always larger than H_{EC}. During the days when the contributions of the mulberry seedling field to the two systems were close to each other, the sensible heat flux measurements of the two instruments were similar. The case analysis on typical sunny days showed that there would be larger sensible heat fluxes over the mulberry seedling field than in the rice paddy field especially under larger net radiation conditions.

Keywords: large aperture scintillometer; sensible heat fluxes; heterogeneous farmland; footprint

1. Introduction

Farmland is a typical underlying surface and widely distributed around the world. In China, due to the family contract responsibility system, farmlands are divided into small pieces allocated to different families, and different crops may be planted within different farmland pieces upon the decision of the owners (e.g., Figure 1). Measurement of the sensible heat fluxes over these mixed-crop farmland fields can help to understand the energy distribution, which plays an important role in the local weather, water cycle and climate [1–4].

Traditionally, eddy covariance (EC), which is based on direct measurements of the product of vertical velocity fluctuations (w′) and scalar concentration fluctuations (c′), is considered as the standard method for sensible heat fluxes measurement [5–9]. However, recently, a new instrument,

the large aperture scintillometer (LAS), was used in a number of field experiments and gradually widely used [10–13]. For LAS, sensible heat fluxes are derived from the line-integral of the structure parameter of the refraction index; the average of sensible heat fluxes is obtained over an area formed by the path length of the light beam of the scintillometer and a line in the upwind direction. In contrast to the EC system, the measurement range of LAS is extended to a few kilometers, which coincides with the common resolution of atmospheric numerical models and satellite remote sensing retrievals (i.e., several kilometers). The application of LAS over different surfaces has been evaluated in a number of experiments [11,14–23], and in some of the experiments, the LAS-derived sensible heat fluxes were compared with EC-derived sensible heat fluxes [14–16,20,24–28]. Over either a homogenous or a heterogeneous surface, these studies demonstrated that the fluxes measured by these two methods had a good consistency, and LAS was a reliable method for deriving the sensible heat fluxes over heterogeneous complex topography.

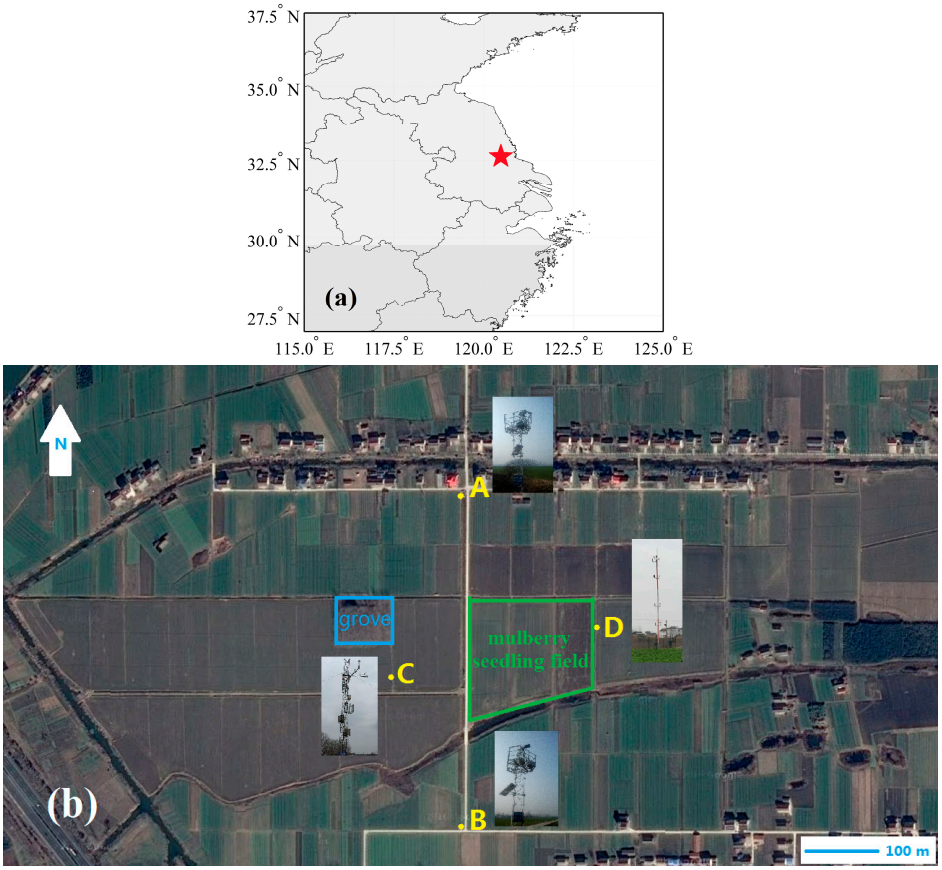

Figure 1. (**a**) Map of eastern China; the location of the experimental site is shown as a red star; (**b**) The experimental site. Points A and B are the transmitter and receiver of the large aperture scintillometer (LAS) with an optical path of 470 m, respectively; C is the eddy covariance (EC) system; and D is the automatic meteorological station (AWS). The mulberry seedling field and grove field are also shown with green and blue frames, respectively. Concrete roads are shown as white bands.

Field experiments were conducted over different farmlands, such as arid grassland [8] and rice paddy [6,29–31], with EC systems over the world. In this study, combined LAS and EC measurements were conducted over the selected heterogeneous farmland in Jiangsu province of China during the period from 13 September–11 October 2015. First, LAS sensible heat fluxes were compared with the EC system here to investigate their reliability and characteristics. Second, average footprints were calculated to analyze the statistical characteristic. Third and the last, the footprint model was used to assess LAS and EC measurements to understand the influence of the heterogeneity in typical sunny

days. It is expected that the results found here will provide a reference for sensible heat fluxes' analysis and/or LAS experiments over heterogeneous farmlands.

The study is organized as follows: Section 2 describes the observational site and micrometeorological measurement systems; Section 3 presents the data processing methods; Section 4 analyzes the results; and Section 5 summarizes and concludes the paper.

2. Observation Site and Micrometeorological Measurement Systems

2.1. Observation Site

The experimental site is at a farmland about 45 km from the east China coast (32.76° N, 120.47° E; 4 m above sea level). The site was generally flat, and around the site, there are some farmhouses (Figure 1). An LAS transmitter unit (marked A in Figure 1), a receiver unit (marked B in Figure 1), EC instruments (marked C in Figure 1) and an automatic meteorological station (AWS marked D in Figure 1) were installed at the site. At three meters east of the LAS optical path (the A-B line in Figure 1), there is a patch of mulberry seedlings with a north, west and east side length of 175 m, 175 m and 125 m, respectively. Additionally, there is a 70 m × 62 m poplar grove at the west of the LAS optical path (and at the north of the EC system). The rest of the areas are rice paddy fields. The experiment was carried out from 13 September–11 October 2015, and continuous sensible heat fluxes were derived by both the LAS and EC systems. During the observation period, the canopy height increased from 0.5 m–0.6 m for the rice paddy, from 0.15 m–0.4 m for the mulberry seedling field, and it remained about 12 m for the poplars in the grove, respectively.

2.2. Micrometeorological Measurement Systems

2.2.1. Large Aperture Scintillometer

The LAS instrument is manufactured by Rainroot Scientific Limited China (Beijing, China), and it has a similar observation principle to the LAS from Kipp&Zonen, but independently designed [32], and has an aperture diameter (D) of 0.15 m, operating at a near-infrared wavelength of 880 nm. The LAS receiver (marked B in Figure 1) and transmitter unit (marked A in Figure 1) were deployed at a height of 6 m on the tower over the paddy. The electromagnetic radiation was transmitted from north to south with an optical path of 470 m. Such a short path is caused by the limitation of the position of local villagers' houses.

2.2.2. EC System

The EC instruments (marked C in Figure 1) were about 100 m to the west of the LAS optical path, including a H_2O analyzer (LI-7500, LI-COR Biotechnology, Lincoln, NE, USA) and a three-dimensional sonic anemometer (CSAT3, Campbell Scientific Inc., Edmonton, AB, Canada). The instruments were installed on a tower at the height of 10 m, and they measure three-dimensional wind speed components u, v, w, theta, the density of air, etc., at a sampling rate of 10 Hz.

2.2.3. Automatic Meteorological Station

The automatic meteorological station (AWS, marked D in Figure 1) was about 185 m to the east of the LAS optical path. The air temperature, humidity and wind speed sensors were placed at each height (3 m, 5 m, 8 m and 10 m) on the tower. A wind direction sensor was deployed at the height of 10 m. The radiometer, measuring upward and downward short and long wave radiations, was installed at a height of 3 m. Each of these sensors sampled at a rate of 1 Hz, and the measurements were averaged at 30-min intervals.

3. Data Processing Methods

3.1. Parameter Set

The aerodynamic roughness length (z_0) and the zero plane displacement height (d) were calculated through the gradient method with EC and AWS data. Based on the Monin–Obukhov (M–O) similarity hypothesis, the vertical wind profile is expressed as follows:

$$u = \frac{u_*}{\kappa} \ln \frac{z-d}{z_0} - \Psi_m\left(\frac{z-d}{L}\right) + \Psi_m\left(\frac{z_0}{L}\right) \quad (1)$$

where z is the height with respect to wind speed u, L is the Obukhov length derived by EC systems, $\kappa(=0.4)$ is the von Karman constant and u_* is the friction velocity. The integrated stability correction function Ψ_m was given by Dyer [33]:

$$\Psi_m(\xi) = 2\ln(\frac{1+x}{2}) + \ln(\frac{1+x^2}{2}) - 2\arctan x + \frac{\pi}{2} \quad (2)$$

$$x = (1-16\xi)^{\frac{1}{4}} \quad (3)$$

$$\Psi_m(\xi) = -5\xi \quad (4)$$

where Equations (2) and (3) are valid under unstable conditions and Equation (4) is valid under stable conditions. Then, the fitting process was conducted on AWS-measured wind speed data, and the results showed that the mean of z_0 was 0.025 m; and d varied from 0.43 m on 13 September to 0.55 m on 11 October 2015. Besides, owing to the flat underlying surface, the LAS effective height (z_{eff}) was estimated to be its installation height of 6 m.

3.2. Data Process Scheme of EC

In this paper, we used EddyPro 5.2.1 (software developed by LI-COR Biotechnology) to process data measured by the EC system. The EddyPro software applied the following corrections: despiking algorithm [34], spectral corrections [35,36], compensation for density fluctuations [37], time lag compensation, double rotation for tilt correction, block averaging, statistical tests [34], etc. Then, the half-hour averages of heat fluxes were derived. As the sensible and latent heat fluxes were calculated, the Bowen ratio β could be derived as:

$$\beta = \frac{H_{EC}}{LE_{EC}} \quad (5)$$

where H_{EC} is EC-derived sensible heat fluxes, and LE_{EC} is EC-derived latent heat fluxes. For the missing data or the results that β > 3 (unstable phase) during the observation period, the Bowen ratios were set up as the average β (=0.22). Then β can be used in the calculation of sensible heat fluxes from LAS.

3.3. Scintillometry Method

The intensity of fluctuations in the refractive index of air, which can be converted to the structure parameter of the refractive index (C_n^2) turbulence [38], could indicate the variation of atmosphere turbulence. LAS measures the intensity of optical fluctuations as the laser goes through a turbulent atmosphere. C_n^2 can be expressed as the function of the structure parameter of temperature (C_T^2) and humidity (C_q^2) [39]. Additionally, it is sensitive to the fluctuations of temperature more than humidity at a near-infrared wavelength [40]. Further, Odhiambo and Savage [41] verified that the sensible heat fluxes derived from the surface layer scintillometry (one kind of scintillometer that is similar to LAS in sensible heat fluxes' measurements between 50 and 350 m) with the β-corrected C_T^2 has

greater agreement with the EC-derived sensible heat fluxes than that without β correction. Following Odhiambo and Savage [41], C_n^2 is expressed as:

$$C_n^2 = C_T^2\left(\frac{-0.78\times10^{-6}P}{T^2}\right)^2\left(1+\frac{0.03}{\beta}\right)^2 \tag{6}$$

where T is the air temperature (K), P is the atmospheric pressure (Pa) and β is the Bowen ratio derived from EC. Normally, the Bowen ratios were smaller than 1 (mean of 0.22 for this study) under rice paddy. The calculated C_T^2 could overestimate about 30% without the Bowen ratio correction. Therefore, this correction could not be neglect in this paper. The half-hourly average C_n^2 was calculated to match the averaging period of EC, and the noise was eliminated by using a criterion of $X(t) < \overline{X} - 4\sigma$ or $X(t) > \overline{X} + 4\sigma$, where $X(t)$ is the measurement, $\overline{X}$ is the mean over the interval and σ is the standard deviation. Besides, the mathematical relationship of C_n^2 and the variance of the natural logarithm of light intensity was not established, and the measurement should be eliminated when the LAS signal is saturated (with higher turbulence intensity). Based on Ochs and Hill [42], the threshold value of C_n^2 for LAS signal saturation is set to $5.87 \times 10^{-12}\mathrm{m}^{-2/3}$ in our experiment.

Then, according to the M-O similarity hypothesis, the following equation can be derived:

$$\frac{C_T^2(z_{eff}-d)^{\frac{2}{3}}}{T_*^2} = f_T\left(\frac{z_{eff}-d}{L}\right) \tag{7}$$

where T_* is the surface layer temperature scale parameter, z_{eff} is the LAS effective height, d is the zero plane displacement, L is the Obukhov length and f_T is a universal dimensionless function of the temperature structure parameter. Several forms of f_T have been proposed from different experiments [43–49]. This paper adopts the function of Andreas (1988) [45]:

$$f_T\left(\frac{z_{eff}-d}{L}\right) = 4.9\left(1-6.1\frac{z_{eff}-d}{L}\right)^{-\frac{2}{3}} \text{ for the unstable condition,} \tag{8}$$

$$f_T\left(\frac{z_{eff}-d}{L}\right) = 4.9\left(1+2.2\left(\frac{z_{eff}-d}{L}\right)^{\frac{2}{3}}\right) \text{ for the stable condition.} \tag{9}$$

The friction velocity u_* and the Obukhov length L were calculated as:

$$u_* = \frac{\kappa u}{\ln\frac{z_{eff}-d}{z_0} - \Psi_m\left(\frac{z_{eff}-d}{L}\right) + \Psi_m\left(\frac{z_0}{L}\right)} \tag{10}$$

$$L = \frac{u_*^2 T}{gkT_*} \tag{11}$$

where $\kappa(=0.4)$ is the von Karman constant, and $g(=9.8\ \mathrm{m\ s^{-2}})$ is the acceleration of gravity. u is the wind speed at the height of z_{eff}. Owing to the different heights of LAS and EC, u was obtained through neutral-condition log-law correction of the EC-measured wind speed.

The surface layer is considered as unstable when these following inequalities were satisfied:

$$\begin{cases} H_{EC} > 0\ \mathrm{W\ m^{-2}} \\ R_n > 10\ \mathrm{W\ m^{-2}} \end{cases} \tag{12}$$

where R_n is net radiation. The surface layer parameters T_*, u_* and L are solved using an iterative calculation of Equations (2)–(4) and (6)–(11), then area-averaged H_{LAS} can be calculated through the T_* (based on C_n^2) and u_* (sensitive to the local roughness):

$$H_{LAS} = -\rho C_P u_* T_* \tag{13}$$

where ρ is the air density and C_P is the specific heat capacity of air at constant pressure. Similar to Gruber and Fochesatto [50], the convergence of this iterative calculation was identified through the fixed-point method [50]. Combining Equations (2)–(4) and (6)–(11), the recursive function was:

$$\frac{z_{eff}-d}{L} = M\frac{\left(\ln\frac{z_{eff}-d}{z_0} - \Psi_m\left(\frac{z_{eff}-d}{L}\right) + \Psi_m\left(\frac{z_0}{L}\right)\right)^2}{f_T\left(\frac{z_{eff}-d}{L}\right)^{1/2}} \tag{14}$$

where under unstable conditions:

$$M = -\frac{g\left(z_{eff}-d\right)\sqrt{C_T^2\left(z_{eff}-d\right)^{2/3}}}{T\kappa u^2} \tag{15}$$

Equation (14) using fixed-point recursion under unstable conditions is seen in Figure 2. As the relationship of M and $\left(z_{eff}-d\right)/L$ is monotonic, the iterative calculation was applicable to derive sensible heat fluxes from LAS measurement under unstable conditions.

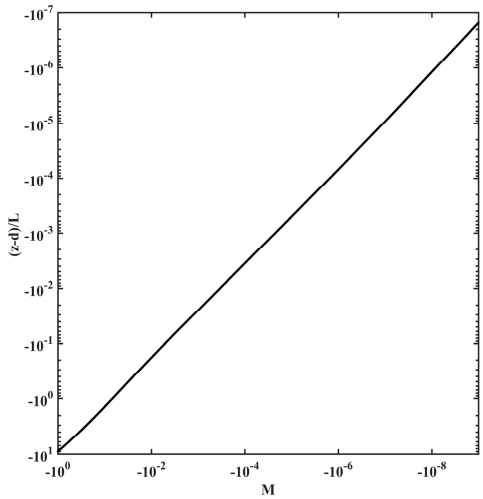

Figure 2. Solution of Equation (14) using fixed-point recursion, and the relationship of M and $\left(z_{eff}-d\right)/L$ is monotonic.

3.4. Calculation Uncertainty

The uncertainty of EC-derived sensible heat fluxes was also calculated through Finkelstein and Sims' [51] method; the results under unstable conditions are shown in Figure 3a with the increase of H_{EC}; the uncertainty of H_{EC} could increase from almost zero to about 17 W m^{-2}; and the mean uncertainty was 5.46 W m^{-2}.

Even if turbulence is being sampled above an extremely flat field, for LAS, the uncertainty in z will still be present. The uncertainty of LAS should be assessed before comparison. The sensitivity function for the sensible heat flux H_{LAS} under unstable conditions was given by Gruber et al. [52]:

$$S_{H,z} = \frac{\begin{array}{c} -z(u)(z(u)+6.1z(u)^2\breve{\Lambda}(6.1\zeta^2-\zeta)^{1/4})^{-5/3} \\ \cdot(1+12.2z(u)\breve{\Lambda}(6.1\zeta^2-\zeta)^{1/4})G(u) \end{array}}{\left\{\left[\int_0^1 (z(u)+6.1z(u)^2\breve{\Lambda}(6.1\zeta^2-\zeta)^{1/4})^{-2/3}G(u)\mathrm{d}u\right]\right.} \\ +6.1\breve{\Lambda}(6.1\zeta^2-\zeta)^{1/4}\cdot\left[\int_0^1 (z(u)+6.1z(u)^2\breve{\Lambda}(6.1\zeta^2-\zeta)^{1/4})^{-5/3}z(u)G(u)\mathrm{d}u\right] \\ \left.-\frac{4(6.1\zeta^2-\zeta)^{3/4}}{\breve{\Lambda}}\cdot\left[\int_0^1 (z(u)+6.1z(u)^2\breve{\Lambda}(6.1\zeta^2-\zeta)^{1/4})^{-2/3}G(u)\mathrm{d}u\right]^{5/2}\right\} \quad (16)$$

$$\zeta = \frac{z-d}{L} \quad (17)$$

$$\breve{\Lambda} = \left(\frac{\kappa g\sqrt{C_T^2}}{u_*^2 T\sqrt{4.9}}\right)^{3/4} \quad (18)$$

where $z(u)$ is the height of the beam along the relative path position u. The weight function from Hartogensis et al. [53] is as follow:

$$G(u) = 16\pi^2K^2L\int_0^\infty k\phi_n(k)\sin^2\left[\frac{k^2Lu(1-u)}{2K}\right]\cdot\left[\frac{2J_1(x_1)J_2(x_2)}{x_1x_2}\right]^2\mathrm{d}k \quad (19)$$

where L is the optical path length, $K = 2\pi/\lambda$ is the optical wavenumber, k the turbulent spatial wavenumber, $\phi_n(k) = 0.033k^{11/3}$ the three-dimensional spectrum of the refractive index in the inertial range and $J_1(x_1)$ and $J_2(x_2)$ are Bessel functions of the first kind, first order with $x_1 = kDu/2$ and $x_2 = kD(1-u)/2$, where D is the aperture diameter. Combining Equations (16)–(19), the uncertainty of LAS-derived sensible heat fluxes could be calculated through:

$$\sigma_H = H_{LAS}\int_0^1 \frac{\sigma_z(u)}{z(u)}S_{H,z}\mathrm{d}u \quad (20)$$

where $\sigma_z(u)$ is the uncertainty of z through relative path position u. With the zero plane displacement height varied from 0.43–0.55 m, the difference of 0.12 m may indicate the uncertainty of z. The uncertainty of LAS-derived sensible heat fluxes is shown in Figure 3b with the mean of 0.74 W m^{-2}.

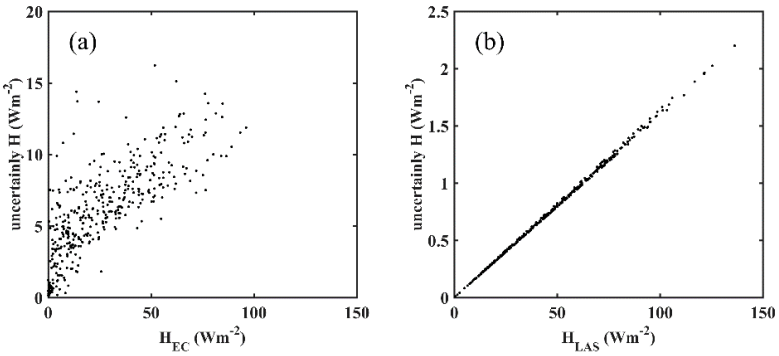

Figure 3. Uncertainty of (**a**) EC- and (**b**) LAS-derived sensible heat fluxes from measurements during this observation period.

3.5. Footprint Analysis

The flux footprint provides a means of estimating both the source area and the relative contribution of each surface element to the measured fluxes. In this paper, the flux footprint model was calculated through [54]:

$$f_{LAS} = \int_{x_1}^{x_2} G(u) f(x - x', y - y', z) \mathrm{d}x \tag{21}$$

where $G(u)$ is the weight function and x_1 and x_2 are the position of transmitter and receiver of LAS, respectively. (y) and $x'(y')$ are the point in the optical path and in the up-wind areas, respectively. f is the point-flux footprint model from Kormann and Meixner [55].

4. Results

4.1. Meteorological Conditions

Temporal variations of wind speed, air temperature, relative humidity, surface atmospheric pressure and precipitation from 12 September to 11 October 2015 was showed in Figures 4 and 5. During the observation period, the wind speed (WS) showed obvious diurnal variation, and the maximum WS occurred at noon every day with a value varying from 1.95–10 m s^{-1} on different days (Figure 4a). Between the height of 10 m and 3 m, the WS difference was always less than 1 m s^{-1}. The overall average WS was 2.43 m s^{-1} at 10 m, 2.21 m s^{-1} at 8 m, 1.94 m s^{-1} at 5 m and 1.72 m s^{-1} at 3 m, respectively. The highest value of WS was 10 m s^{-1} at the height of 10 m at 10:30 on 29 September. Combined with Figure 5, it is easy to find that the prevailing winds were easterlies at the observation height of 10 m in this site. During the daytime, more than 62 percent of winds were easterlies (including southeasterlies and northeasterlies), and only 21 percent of winds were westerlies (including southwesterlies and northwesterlies). At night, about 51 percent of winds were from the east, and 26 percent were from the west. The air temperature (Figure 4b) also significantly varied with a diurnal cycle. Most of the values were between 283 K and 298 K, and the overall average air temperature was 291.62 K at 10 m, 291.75 K at 8 m, 291.95 K at 5 m and 292.03 K at 3 m, respectively. As the height increased, the air temperature slightly decreased, but the temperature difference between the highest and lowest levels was less than 0.5 K at daylight. Driven by the variation of the surface net radiation, the highest and lowest temperature often occurred at 14:00 and 2:00, respectively. The maximum and minimum temperatures were 298.17 K and 283.88 K (caused by a strong precipitation process) at 14:30 on 18 September and at 5:30 on 2 October, respectively. Relative humidity (RH) also varied largely between mostly 50% and 100% during a day. Generally, the maximum RH (Figure 4c) followed the minimum air temperature at about 2:00, while the minimum RH corresponded to the maximum air temperature at about 14:00. It is noteworthy that RH was also influenced by other factors such as precipitation, advective flow, transpiration and turbulent intensity. The variation of atmospheric pressure is presented in Figure 4d. During the observation period, the value of atmospheric pressure varied from 1020.92 hPa (at 9:30 on 13 September) to 1006.44 hPa (at 12:30 on 23 September) and then increased to 1019.86 hPa (at 10:30 a.m. on 29 September). Later, because the air mass transited from northwest, the pressure went sharply down to 1005.18 hPa (at 4:00 a.m. on 1 October) and finally picked up to 1025.19 hPa (at 9:30 a.m. on 4 October). Combined with the wind speed and wind direction from 29 September–1 October, it could be found that a low pressure moved from west to the east of the site. Meanwhile, the values of pressure varied significantly and had two maximums and minimums during the diurnal cycle. The first low value and high value were usually at about 3:00 a.m. and 10:00 a.m.; the second low value and high value were usually at about 14:00 and 20:00. The temporal variation of precipitation is shown in Figure 4e; there were four obvious precipitation processes: 22–23 September (32.9 mm), 29 September (24.3 mm), 30 September–1 October (34.3 mm) and 7–8 October (4.5 mm).

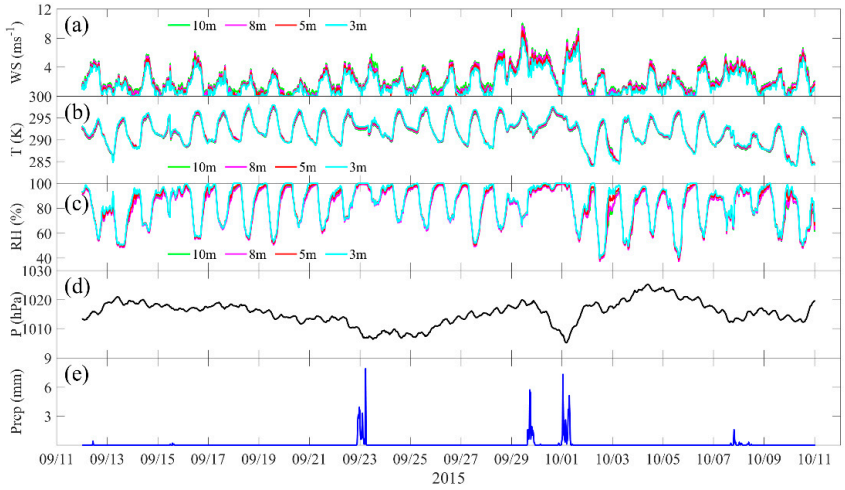

Figure 4. Temporal variations of (**a**) wind speed at 3-, 5-, 8- and 10-m heights (lines); (**b**) air temperature at 3-, 5-, 8- and 10-m heights; (**c**) relative humidity at 3-, 5-, 8- and 10-m heights; (**d**) surface atmospheric pressure and (**e**) precipitation from 12 September–11 October 2015.

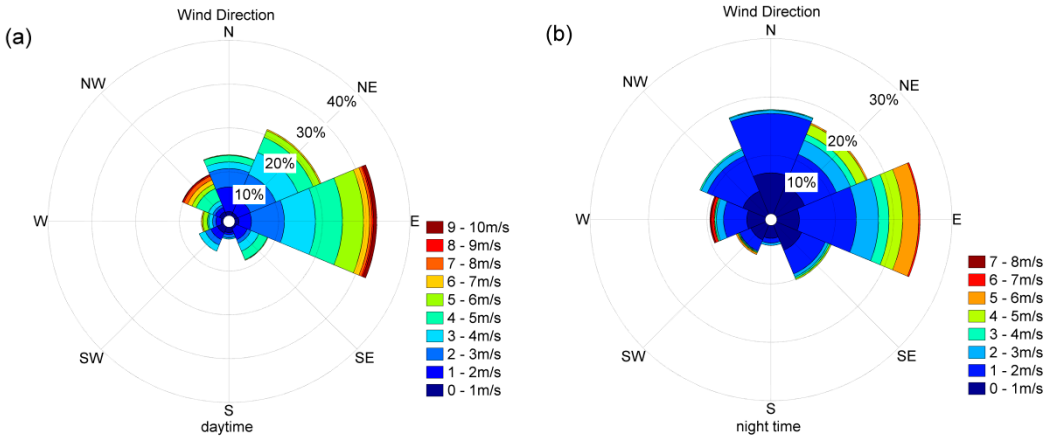

Figure 5. Distributions of (**a**) wind directions at 10-m height during the daytime and (**b**) wind directions at 10-m height during nighttime.

4.2. Turbulent Heat Fluxes

The variations of H_{LAS}, H_{EC}, LE_{EC} and net radiation (Rn) are shown in Figure 6. The maximum of Rn varied from 200 W m^{-2} (on cloudy days) to near 700 W m^{-2} (on sunny days). The maximum of Rn in this period was 682.3 W m^{-2} at 11:30 on 16 September, and the average of the daily maximum of Rn was 489.3 W m^{-2}. Because of the occurrence of the clouds, there were always some fluctuations near the peak of Rn. The H_{LAS} and H_{EC} varied significantly from very low values to about 130 W m^{-2} and about 90 W m^{-2}, respectively. The values of H_{LAS} were always larger than the corresponding H_{EC}, and the difference is mostly experienced in the central part of the day, while towards the beginning and end of the diurnal cycle, the fluxes converged. Considering the uncertainty of the two systems' derived sensible heat fluxes shown in Figure 3, the uncertainty (<17 W m^{-2} for EC) was always smaller than the difference between LAS and EC shown in Figure 6; this may indicate that the differences are not caused by the uncertainty of two instruments. The maximums of H_{LAS} and H_{EC} were 125.36 W m^{-2} (at 10:30 on 6 October) and 93.36 W m^{-2} (at 14:00 on 10 October), respectively; and the averages of the daily maximum of H_{LAS} and H_{EC} were 80.14 W m^{-2} and 59.84 W m^{-2}, respectively. The same as other experiments [22,56], the sensible heat fluxes had a similar diurnal variation pattern with net

radiation. The LE also showed an evident diurnal variation pattern with the average daily maximum of 383.71 W m^{-2}.

The relationship of H_{LAS} and H_{EC} is shown in Figure 7 with negative values omitted. The red points and the corresponding bars represent the median values binned at 5 W m^{-2} of the H_{EC} interval and the interquartile ranges, respectively. The median of H_{LAS} was 13.09 W m^{-2} greater than the median of H_{EC} on average when H_{EC} was at the range of 0–80 W m^{-2}. For the data where H_{EC} exceeded 80 W m^{-2}, the sample numbers were too small to exactly estimate the relationship between H_{LAS} and H_{EC}. Overall, H_{EC} shows that the sensible heat fluxes varied from 0 to about 80 W m^{-2} on the rice paddy fields in eastern China during the maturity period of rice, and it is similar to the measurement during the rice growth period [31].

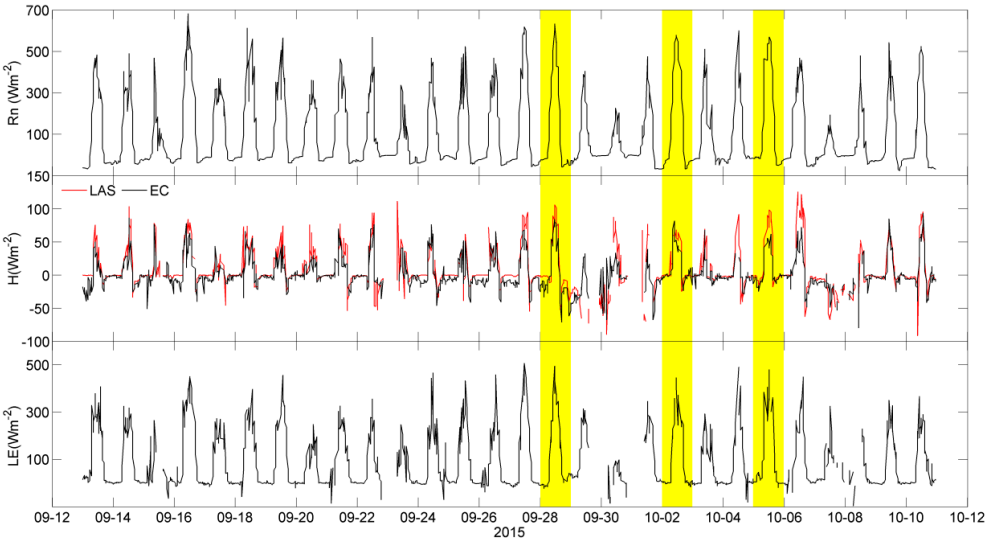

Figure 6. Variations of sensible heat fluxes (H), latent heat fluxes (LE) and net radiation (Rn) from 13 September–11 October 2015. The three days that are discussed in Section 4.3 are marked in yellow.

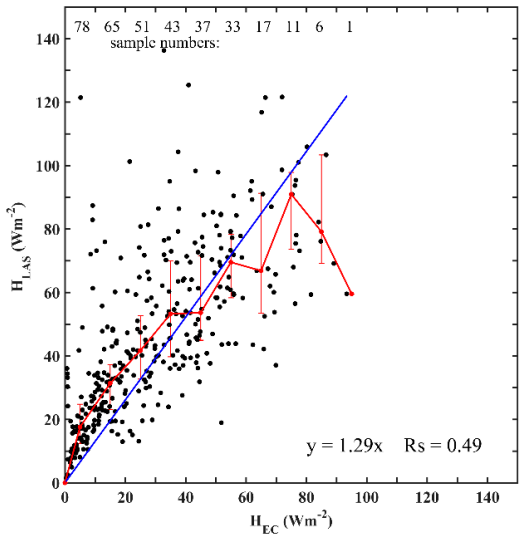

Figure 7. Variations of H_{LAS} and H_{EC} when the sensible heat fluxes were greater than zero from 12 September–11 October 2015. The red points represent the median values binned at 5 W m^{-2} of the interval. The corresponding bars represent the interquartile ranges. The sample numbers are also shown in the figure. The regression lines are plotted in blue. The slopes and determination coefficients are also shown in the picture.

4.3. The Effects of Winds and Associated Footprint on H_{LAS} and H_{EC}

To clarify the reason that H_{LAS} tended to be larger than H_{EC} during the observation period, the effects of wind direction, speed and the associated footprint (the model of Kormann and Meixner [55]) are investigated in this subsection.

Figure 8a–d shows the observed H_{LAS} and H_{EC} under different wind directions, and Figure 8e–h presents the corresponding average footprint under each wind direction condition. Under easterlies, westerlies, southerlies and northerlies, the number of data points is 157, 30, 38 and 116, respectively; and the maximum H_{LAS} (H_{EC}) values are 125.36 (85.56), 95.38 (93.35), 69.51 (81.54) and 84.45 (77.72) W m^{-2}, respectively. The average H_{LAS} (H_{EC}) values are 55.09 (31.96), 50.83 (35.05), 39.59 (27.97) and 33.72 (25.66) W m^{-2}, respectively. The mulberry seedling field contributions to the footprint of H_{LAS} (H_{EC}) are 40.14% (26.66%), 0.07% (0%), 17.31% (0.14%) and 27.23% (1.57%), respectively; while the contributions from the grove field to the footprint of H_{LAS} and H_{EC} are always very small, with a maximum of 4.24% for H_{LAS} and 1.57% for H_{EC} when westerlies prevailed.

It should be noted that the $H_{LAS} - H_{EC}$ regression slope (1.46) was specifically large when easterlies prevailed, while when winds were from other directions, the $H_{LAS} - H_{EC}$ regression slopes were closer to one (1.17, 1.17 and 1.1 for westerlies, southerlies and northerlies, respectively). Therefore, the heterogeneity caused by the mulberry field, which was at the east side of the LAS and EC observation instruments, could play a significant role.

Since the easterlies and northerlies conditions dominated the observation period, the observed sensible heat fluxes and associated mulberry seedling field contributions under the two conditions are analyzed in detail here. First, it is found that when the wind direction switched from northerlies to easterlies, the average H_{LAS} increased from 33.72–55.09 W m^{-2} associated with the average mulberry seedling field contribution from 27.23–40.14%. Second, the average H_{EC} increased from 25.66–31.96 W m^{-2} associated with the average mulberry seedling field contribution from 1.57%–26.66%. Third, similar average mulberry seedling field contributions to LAS under northerlies (27.23%) and to EC under easterlies (26.66%) yielded similar average sensible heat flux observations (33.72 W m^{-2} for LAS and 31.96 W m^{-2} for EC). Based on this evidence, it can be concluded that, under the same meteorological condition and for the same area, the mulberry seedling field generally produces more sensible heat flux than the rice paddy; and the different mulberry seedling field contribution to LAS and EC is the substantial cause of the difference between the H_{LAS} and the H_{EC}.

To clarify the physical mechanism giving the origin to the difference of two instrument under unstable conditions, the factors derived from sensible heat fluxes (shown in Equation (13)) were compared here under north wind and east wind conditions. Under unstable conditions, the LAS-EC regression slope (k), determination coefficient (Rs), mean square error (RMSE) and mean air density (ρ), mean friction velocity (u_*), mean temperature scale parameter (T_*) were calculated (Table 1). First, it is clear that the air density measured from two instruments has a small bias here both under east (1.20 kg m^{-3} for LAS and 1.18 kg m^{-3} for EC) and north wind conditions (1.20 kg m^{-3} for LAS and 1.17 kg m^{-3} for EC). Additionally, the differences were small such that they had a slight influence (less than 3%) on sensible heat fluxes. Second, it is found that when the wind direction switched from northerlies to easterlies, the average u_{*LAS} (u_{*EC}) increased from 0.20 (0.37)–0.26 (0.38) m s^{-1}, and the average T_{*LAS} (T_{*EC}) decreased from −0.16 (−0.067)–−0.21 (−0.079) K associated with the average mulberry seedling field contribution from 27.23% (1.57%)–40.14% (26.66%). Third, under the similar average mulberry seedling field contributions (27.23% for LAS under northerlies and 26.66% for EC under easterlies), the absolute value of average T_{*LAS} was significantly larger than the absolute value of T_{*EC} while u_{*LAS} was smaller than u_{*EC}. This results in a similar value on the average sensible heat flux for two instruments. Therefore, it can be concluded that the mulberry seedling field had significant influence not only on u_*, but also on T_*. The difference of sensible heat fluxes derived from two instruments could be attributed to the different u_* and T_* from the two instruments.

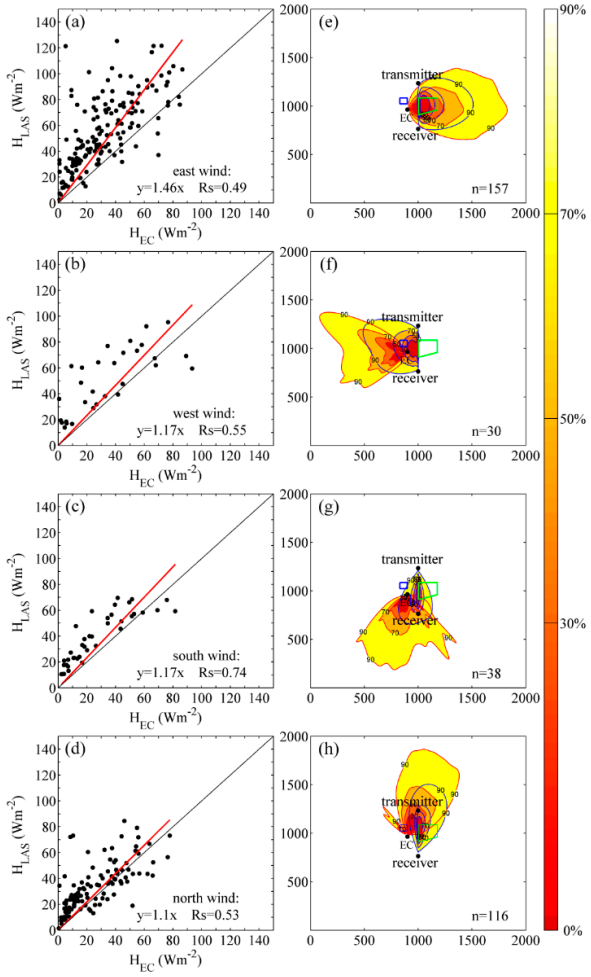

Figure 8. Relationship between LAS-derived and EC-derived sensible heat fluxes under (**a**) east wind; (**b**) west wind; (**c**) south wind and (**d**) north wind conditions is shown in the left panels. The slopes and determination coefficients are also shown in the picture. The regression lines are plotted in red. The corresponding average footprints for LAS and EC under (**e**) east wind; (**f**) west wind; (**g**) south wind and (**h**) north wind conditions are shown in the right panels. The blue rectangle represents the grove, and the green trapezoid represents the mulberry seedling field. The numbers (*n*) of data points are also given in the figure.

Table 1. Comparison of the LAS and EC measured factors derived for sensible heat fluxes under unstable conditions. The LAS-EC regression slope (k), determination coefficient (Rs), mean square error (RMSE), mean air density (ρ), mean friction velocity (u_*), mean temperature scale parameter (T_*) are shown in this table.

Wind Direction	Factors	k	Rs	RMSE	LAS Mean	EC Mean
East	ρ (kg m^{-3})	1.01	0.60	9.82×10^{-5}	1.20	1.18
	u_* (m s^{-1})	0.60	0.20	0.015	0.26	0.38
	T_* (K)	1.97	0.11	0.025	−0.21	−0.079
North	ρ (kg m^{-3})	1.02	0.66	9.13×10^{-5}	1.20	1.17
	u_* (m s^{-1})	0.51	0.41	0.0048	0.20	0.37
	T_* (K)	1.6	0.25	0.013	−0.16	−0.067

RMSE: square error of factors' regression; LAS: averaged measurement from LAS; EC: averaged measurement from EC;

Further, measurements under east and north wind conditions were selected to analyze the influence of wind speeds and the associated footprint. The wind speeds are categorized by 0–2, 2–4

and 4–6 m s^{-1}, while the condition is which wind speeds are larger than 6 m s^{-1} is not considered here due to their infrequent occurrence. For different wind speed conditions under east (north) wind directions, Figure 9a,b shows the observed H_{LAS} and H_{EC}, and Figure 9c–h presents the corresponding averaged footprints. Under easterlies of 0–2, 2–4 and 4–6 m s^{-1}, the footprint extended more eastward when the wind speed increased, and the corresponding contributions of the mulberry seedling field were 53.51% (19.21%), 41.07% (28.25%) and 35.23% (26.71%) for LAS (EC), respectively. Generally, with the increase of the speed of easterlies, the mulberry seedling field contributed less for LAS, but more for EC. When the east winds were at speed of 0–2, 2–4 and 4–6 m s^{-1}; the average H_{LAS} (H_{EC}) were 33.87 (21.50), 47.76 (30.17) and 69.91 (37.69) W m^{-2}, respectively. Following the increasing of wind speed category, the contributions from the mulberry seedling field to LAS and EC became closer to each other, but the difference between the average H_{LAS} and H_{EC} became larger, which was probably caused by the larger sensible heat fluxes' difference over the mulberry seedling field and rice paddies under higher wind speeds and larger average net radiation (the average net radiation was 320.05, 363.24 and 395.75 W m^{-2} for 0–2, 2–4 and 4–6 m s^{-1}).

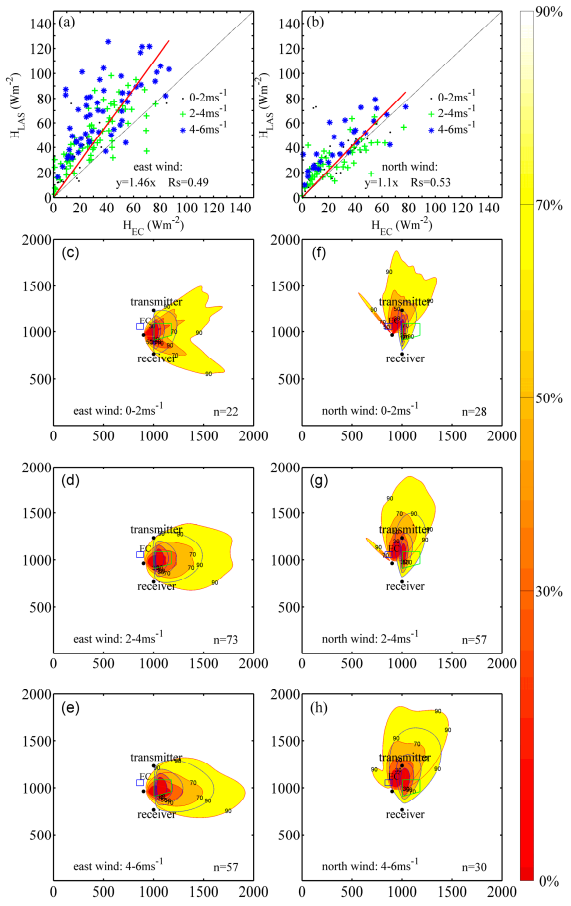

Figure 9. Relationship between LAS-derived and EC-derived sensible heat fluxes under (**a**) east wind and (**b**) north wind conditions. The different wind speed was plotted in black point (0–2 m s^{-1}), green plus sign (2–4 m s^{-1}) and blue asterisk (4–6 m s^{-1}). The slopes and determination coefficients were also shown in the picture. The regression lines were plotted in red. The corresponding average footprints when east wind was 0–2 m s^{-1} (**c**), 2–4 m s^{-1} (**d**) and 4–6 m s^{-1} (**e**). The corresponding average footprints when north wind was 0–2 m s^{-1} (**f**), 2–4 m s^{-1} (**g**) and 4–6 m s^{-1} (**h**). The blue rectangle represents the grove, and the green trapezoid represents the mulberry seedling field. The numbers (n) of data points are also given in the figure.

Under northerlies, the footprint extended northward with the wind speed increase. The contributions of the mulberry seedling field were 36.41% (1.03%), 27.66% (1.24%) and 22.09% (2.28%) for LAS (EC) with wind speed increasing from 0–2 to 4–6 m s^{-1}. When the north winds were at speeds of 0–2, 2–4 and 4–6 m s^{-1}, the average net radiation was 281.92, 291.74 and 362.09 W m^{-2}, respectively. Additionally, the average H_{LAS} (H_{EC}) were 32.39 (23.08), 27.78 (23.81) and 44.54 (30.91) W m^{-2}, respectively. The results show that the larger mean net radiation also corresponds to the higher wind speed.

4.4. Case Analysis

The sensible heat fluxes vary under different weather conditions (net radiation, wind, etc.) during the observation period (Figure 6). To investigate the mechanisms of the fact that H_{LAS} were inclined to be larger than H_{EC}, three typical sunny days (28 September, 2 and 5 October, marked as yellow in Figure 6) were selected to analyze the possible impact of the varied wind conditions (i.e., direction and speed) on the measured sensible heat fluxes. During the three days, the daily variation of net radiation was similar, so that the impact of net radiation on sensible heat fluxes could be omitted. Besides, LAS and EC measurements can have higher reliability when the values of sensible heat fluxes are relatively large under the free convective conditions. Therefore, only the data collected between 10:00 and 15:00 were used here, and the EC system measurements were very low depending on where it was placed compared to the core of the thermal motion during this time period. During 10:00 and 15:00 on the three days, Rn, H_{LAS} and H_{EC} were always larger than 400, 50 and 30 W m^{-2}, respectively. The 10:00–15:00 averages of net radiation (Rn_{avg}), latent heat fluxes (LE_{avg}), wind speed (WS_{avg}) and sensible heat fluxes (H_{LASavg} and H_{ECavg}) were calculated (Table 2). Further, with the footprint model of Kormann and Meixner [55], the averages of the mulberry seedling field contributions for LAS ($K_{LASmavg}$) and EC (K_{ECmavg}) measurements during 10:00 and 15:00 were calculated based on their weighted area proportions of the calculated footprint source area.

Table 2. Comparison of temporal mean (10:00–15:00) LAS-derived and EC-derived sensible heat fluxes with different weather and footprint conditions on some sunny days. The mean value of net radiation (Rn_{avg}), latent heat fluxes (LE_{avg}), wind speed (WS_{avg}), wind direction (WD), LAS- and EC-derived sensible heat fluxes (H_{LASavg} and H_{ECavg}) and the contribution of the mulberry seedling field for the LAS and EC systems ($K_{LASmavg}$ and K_{ECmavg}) are shown in the table.

Date	Rn_{avg}	LE_{avg}	WS_{avg}	WD	H_{LASavg}	H_{ECavg}	$K_{LASmavg}$	K_{ECmavg}
	(W m^{-2})	(W m^{-2})	(m s^{-1})	-	(W m^{-2})	(W m^{-2})	-	-
28 September	499.74	360.77	5.68	East	79.92	60.79	33.78%	36.05%
2 October	497.95	350.06	3.12	West	55.24	47.03	3.06%	0%
5 October	494.84	364.84	2.91	East	76.12	41.64	45.15%	21.92%

4.4.1. Effects of Different Wind Directions

2 and 5 October were chosen to distinguish the effects of different wind directions on the sensible heat fluxes, because the values of Rn_{avg}, LE_{avg} and WS_{avg} on the two days were very similar to each other, but not the WD (Table 2). Table 2 shows that H_{LASavg} was larger than H_{ECavg} on 5 October, but close to H_{ECavg} on 2 October, and the LAS-measured sensible heat fluxes were larger on 5 October than on 2 October. Figure 10a,b further confirms that on 5 October, H_{LAS} was always larger than H_{EC}, while on 2 October, their variations were similar to each other. During the two days (2 and 5 October), the calculated footprint areas were at the west and east of the instruments, respectively (Figure 10c,d). Please be reminded that there was a mulberry seedling field at the east of the optical path (green trapezoid in Figure 10c,d) and a poplar grove at the west (blue rectangle in Figure 10c,d). The grove contributed little during the two days; footprint analysis shows that the contribution of the grove to H_{LAS} or H_{EC} was smaller than 1.5%. However, during 10:00–15:00 on 2 and 5 October, the mulberry seedling field contributed 3.06% and 45.15% to H_{LAS}, 0% and 21.92% to H_{EC}, respectively. In other

words, on 2 October, H_{LAS} and H_{EC} were generally from the homogenous rice paddies; while on 5 October, the mulberry seedling field affected H_{LAS} and H_{EC} greatly, and the influence was different for the two instruments. Generally, under the same meteorological condition (i.e., wind, downward short and long wave radiation), the sensible heat fluxes were homogeneous over a uniform underlying surface such as a rice paddy field [18], which is supported by the observation on 2 October when the footprints of LAS and EC were both over the rice paddy field. However, when the footprints of LAS covered more the mulberry seedling field than that of EC on 5 October, H_{LAS} and H_{EC} diverged drastically. On 5 October, based on the fact that the mulberry seedling field accounted for more weight in footprints for LAS than that for EC, it can be concluded that the mulberry seedling field contributed more sensible heat fluxes to LAS than that to EC. On the other hand, on 5 October, the H_{LAS} was larger than H_{EC}, while it can be further deduced that the mulberry seedling field generated more sensible heat fluxes than that rice paddy field. Therefore, due to the influence of the mulberry seedling field at the east side of the instruments, the sensible heat fluxes obtained by LAS were generally larger on the days with easterlies than on the days with westerlies. Alfieri and Blanken [57] found that a single point measurement (EC systems) is not sufficient to accurately describe this sand-sagebrush environment where the components of the surface energy budget can differ substantially across short distances. Meanwhile, EC could not capture the large-scale motions, which were beyond its footprint [58]. The difference between LAS and EC might have been caused by the large-scale turbulence at the experimental site.

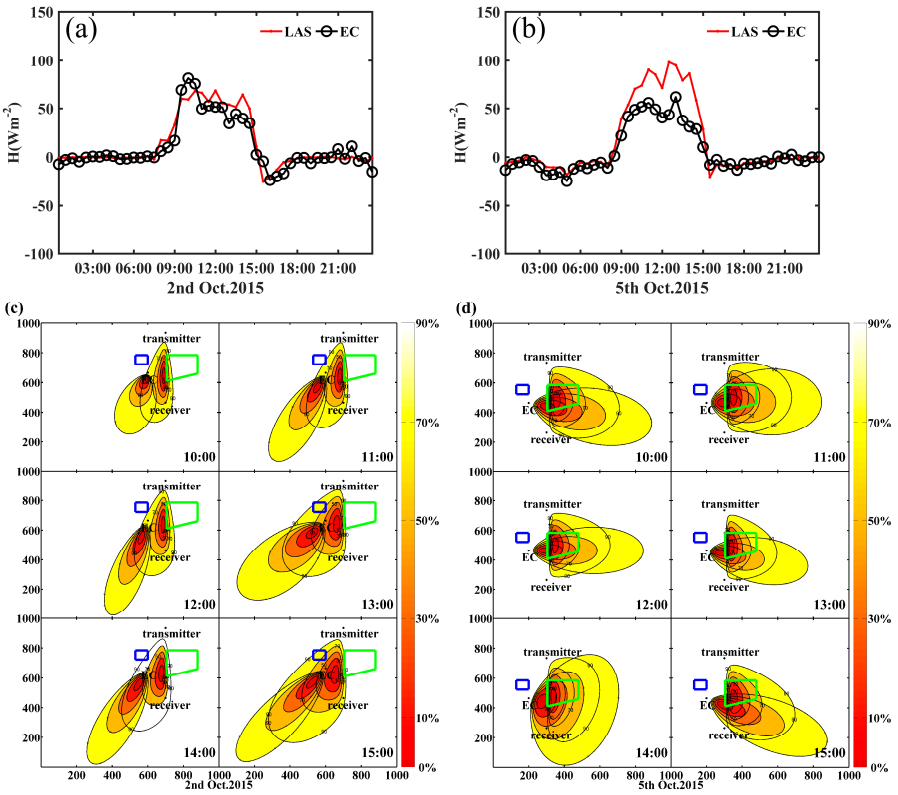

Figure 10. Variations of H_{LAS} and H_{EC} on 2 (**a**) and 5 October (**b**). Footprints of sensible heat fluxes measured by EC and LAS systems on 2 October (**c**), and on 5 October (**d**). The blue rectangle represents the grove field, and the green trapezoid represents the mulberry seedling field. Additionally, the corresponding time is marked in the lower right corner of picture.

4.4.2. Effects of Different Wind Speed

28 September and 5 October were chosen to distinguish the effects of different wind speeds on the sensible heat fluxes, because the values of Rn_{avg}, LE_{avg} and WD in the two days were very similar to each other, but not WS_{avg} (Table 2). Table 2 shows that H_{LASavg} was larger than H_{ECavg} not only on 28 September but also on 5 October, and the sensible heat fluxes obtained by the two instruments were larger on 28 September than on 5 October. Figure 11a,b further confirms that H_{LAS} was always larger than H_{EC} on 28 September and 2 October, but their differences decreased with larger wind speeds. During the two days (28 September and 5 October), the calculated footprint areas are both at the east of the instruments (Figures 10d and 11b). Still, there was the mulberry seedling field at the east of the optical path (green trapezoid in Figures 10d and 11b). During 10:00–15:00 on 28 September and 5 October, the mulberry seedling field contributed 33.78% and 45.15% to H_{LAS}, 36.05% and 21.92% to H_{EC}, respectively. Generally, the sensible heat fluxes were homogeneous over the rice paddy field (discussed above). Meanwhile, for EC, the mulberry seedling field contributed more sensible heat fluxes on 28 September than on 5 October, and EC obtained larger values on 28 September. Therefore, it can be reconfirmed that the mulberry seedling field generates more sensible heat fluxes than that rice paddy field. Due to the influence of the mulberry seedling field at the east side of the instruments, the sensible heat fluxes obtained by EC were increased while LAS-derived sensible heat fluxes were almost invariable under greater wind speeds conditions when the weather was dominated by prevailing easterly wind. Due to the influence of the mulberry seedling field at the east side of the instruments, the sensible heat fluxes obtained by EC were increased while LAS-derived sensible heat fluxes were almost invariable under larger wind speeds conditions when the weather was dominated by prevailing easterly wind. The different phenomenon of LAS and EC might be caused by the difference of the measurement theory between two instruments. The LAS-derived sensible heat fluxes are based on M-O similarity equations; while EC measured turbulence directly and required a certain level of mechanical turbulence present in the flow. The error by using M-O similarity equations under a heterogeneous underlying surface may affect the accuracy of the LAS-derived sensible heat fluxes, and the EC measurement under low wind conditions may also be erroneous.

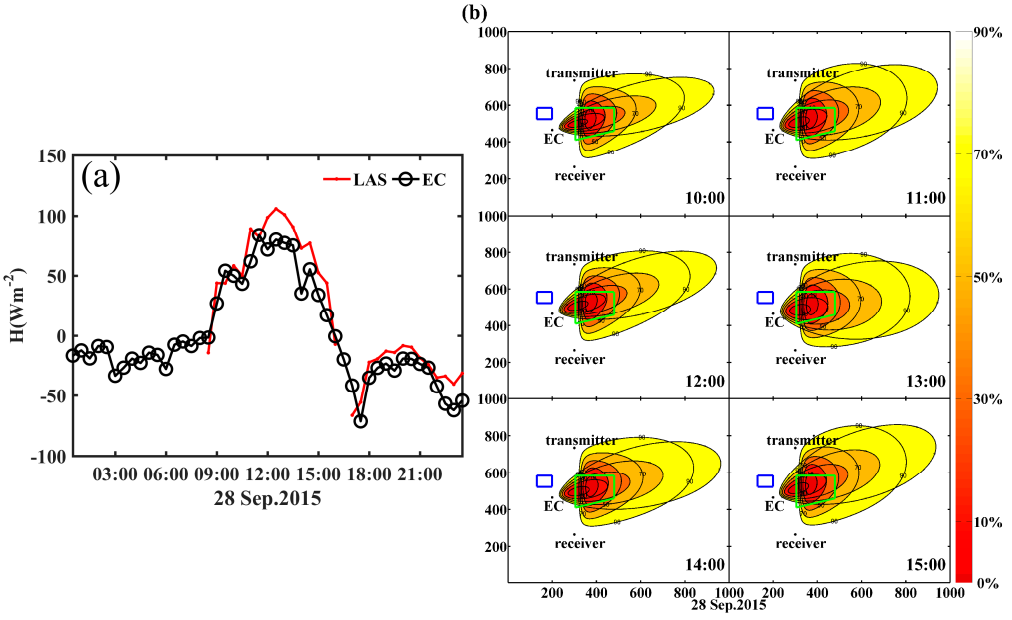

Figure 11. Variations of H_{LAS} and H_{EC} on 28 September were shown in (**a**,**b**) Footprints of sensible heat fluxes measured by the EC and LAS systems on 28 September. The blue rectangle represents the grove, and the green trapezoid represents the mulberry seedling field. Additionally, the corresponding time is marked in the lower right corner of picture.

5. Conclusions

This study compared sensible heat fluxes measured by a large aperture scintillometer and an eddy covariance system over a rice paddy in the coastal region of east China during the period from 13 September–11 October 2015. Through the comparison of the two sets of data, it can be found that the majority of the values of H_{LAS} were larger than H_{EC}, and the daily maximum of H_{LAS} (H_{EC}) during the period was about 100 (80) W m^{-2}.

First, the daytime sensible heat fluxes and corresponding average footprints under different wind direction conditions were compared. During the observation period, east wind and north wind prevailed, and the footprint analysis showed that under larger contribution conditions of the mulberry seedling field, the average H_{LAS} was always larger than H_{EC}. The consistent measurements of sensible heat fluxes by the two instruments often correspond to the consistent contributions from the mulberry seedling field for the two instruments' source areas. That is, the mulberry seedling field has significantly affected the sensible heat fluxes' observation of the two systems, and the influence is not only on u_*, but also on T_*. The difference of the sensible heat fluxes derived from the two instruments could be attributed to the different u_* and T_* from the two instruments.

Under easterlies and northerlies, with increasing wind speed, which always corresponded to larger net radiation, the footprint extended more eastward and northward, respectively; and the mulberry seedling field's contributions to the two instruments became more similar to each other; but the difference between H_{LAS} and H_{EC} became larger. It is also concluded that the difference of the sensible heat fluxes over the mulberry seedling field and over rice paddies increased with the average net radiation conditions.

Finally, the H_{LAS} was generally larger under easterlies than under westerlies conditions. Footprint analysis showed that, under easterlies, the source areas of instrument were rice paddies together with a mulberry seedling field. Additionally, under westerlies, the source areas were basically rice field. This confirmed that the sensible heat fluxes over the mulberry seedling field were larger than the value over the rice paddies field. For LAS, the contribution of the mulberry seedling field was larger, and that made the LAS-derived sensible heat fluxes larger than those that were EC derived on east wind conditions. Through the comparison of sensible heat fluxes measured by the two instruments under different east wind speed conditions, it is found that under east wind conditions, the enlargement of H_{EC} is consistent with the increasing contribution of the mulberry seedling field for EC. This confirms that there were larger sensible heat fluxes over the mulberry seedling field than over the rice paddy again.

This paper found that during the observation period, the sensible heat fluxes over the mulberry seedling field were larger than over the rice paddy field especially under larger net radiation conditions. Additionally, the heterogeneity caused by the different crops in nearby fields played an important role in the sensible heat fluxes' observation by the LAS and EC systems. This paper shows an example of using the two observation systems (LAS and EC) to expose the effect of surface heterogeneity. More detailed analysis of the variation of sensible heat fluxes over each kind of crop in east China will be carried out with further observation experiments.

Acknowledgments: This study is supported by the National Natural Science Foundation of China under Grants 41475085, 41275022, 41505004 and 41675009, the National Program on Key Basic Research Project of China (973) under Grant 2012CB417203, and the National Key Project of MOST under Grant JFYS2016ZY01-002213.

Author Contributions: Zhiqiu Gao and Yubin Li conceived of and designed the experiments. Xin Li and Bing Tong performed the experiments. Zhiqiu Gao and Yubin Li proposed the idea. Xin Li processed the data and wrote the first draft. Zhiqiu Gao, Yubin Li and Xin Li participated in the revision.

Conflicts of Interest: The authors declare no conflict of interest.

References

1. Liang, L.; Lu, S.; Shang, L. Numerical simulation of effect of loess plateau vegetation change on local climate. *Plateau Meteorol.* **2008**, *27*, 293–300.
2. Pielke, R.A. Influence of the spatial distribution of vegetation and soils on the prediction of cumulus convective rainfall. *Rev. Geophys.* **2001**, *39*, 151–177. [CrossRef]
3. Foley, J.A.; DeFries, R.; Asner, G.P.; Barford, C.; Bonan, G.; Carpenter, S.R.; Chapin, F.S.; Coe, M.T.; Daily, G.C.; Gibbs, H.K. Global consequences of land use. *Science* **2005**, *309*, 570–574. [CrossRef] [PubMed]
4. Findell, K.L.; Shevliakova, E.; Milly, P.; Stouffer, R.J. Modeled impact of anthropogenic land cover change on climate. *J. Clim.* **2007**, *20*, 3621–3634. [CrossRef]
5. Bian, L.; Gao, Z.; Xu, Q.D.; Lu, L.H.; Yanjie, C. Measurement of turbulence transfer in the near-surface layer over the southeastern tibetan plateau. *Bound. Layer Meteorol.* **2002**, *102*, 281–300. [CrossRef]
6. Gao, Z.; Bian, L.; Zhou, X. Measurements of turbulent transfer in the near-surface layer over a rice paddy in China. *J. Geophys. Res. Atmos.* **2003**. [CrossRef]
7. Gao, Z.; Lenschow, D.H.; Horton, R.; Zhou, M.; Wang, L.; Wen, J. Comparison of two soil temperature algorithms for a bare ground site on the loess plateau in China. *J. Geophys. Res. Atmos.* **2008**. [CrossRef]
8. Bi, X.; Gao, Z.; Deng, X.; Wu, D.; Liang, J.; Zhang, H.; Sparrow, M.; Du, J.; Li, F.; Tan, H. Seasonal and diurnal variations in moisture, heat, and CO_2 fluxes over grassland in the tropical monsoon region of southern China. *J. Geophys. Res. Atmos.* **2007**. [CrossRef]
9. Bi, X.; Gao, Z.; Liu, Y.; Liu, F.; Song, Q.T.; Huang, J.; Mao, W.K.; Chunxia, L. Observed drag coefficients in high winds in the near offshore of the south china sea. *J. Geophys. Res. Atmos.* **2015**, *120*, 6444–6459. [CrossRef]
10. Kleissl, J.; Hartogensis, O.K.; Gomez, J.D. Test of scintillometer saturation correction methods using field experimental data. *Bound. Layer Meteorol.* **2010**, *137*, 493–507. [CrossRef]
11. Evans, J.G.; McNeil, D.D.; Finch, J.W.; Murray, T.; Harding, R.J.; Ward, H.C.; Verhoef, A. Determination of turbulent heat fluxes using a large aperture scintillometer over undulating mixed agricultural terrain. *Agric. For. Meteorol.* **2012**, *166–167*, 221–233. [CrossRef]
12. McGloin, R.; McGowan, H.; McJannet, D.; Cook, F.; Sogachev, A.; Burn, S. Quantification of surface energy fluxes from a small water body using scintillometry and eddy covariance. *Water Resour. Res.* **2014**, *50*, 494–513. [CrossRef]
13. Lee, S.-H. Determination of turbulent sensible heat flux over a coastal maritime area using a large aperture scintillometer. *Bound. Layer Meteorol.* **2015**, *157*, 309–319. [CrossRef]
14. Bruin, H.A.R.D.; Hurk, B.J.J.M.V.D.; Kohsiek, W. The scintillation method tested over a dry vineyard area. *Bound. Layer Meteorol.* **1995**, *76*, 25–40. [CrossRef]
15. Anandakumar, K. Sensible heat flux over a wheat canopy optical scintillometer measurements and surface renewal analysis estimations. *Agric. For. Meteorol.* **1999**, *96*, 145–156. [CrossRef]
16. Cain, J.D.; Rosier, P.T.W.; Meijninger, W.; Bruin, H.A.R.D. Spatially averaged sensible heat fluxes measured over barley. *Agric. For. Meteorol.* **2001**, *107*, 307–322. [CrossRef]
17. Bouin, M.N.; Legain, D.; Traullé, O.; Belamari, S.; Caniaux, G.; Fiandrino, A.; Lagarde, F.; Barrié, J.; Moulin, E.; Bouhours, G. Using scintillometry to estimate sensible heat fluxes over water: First insights. *Bound. Layer Meteorol.* **2012**, *143*, 451–480. [CrossRef]
18. Ward, H.C.; Evans, J.G.; Grimmond, C.S.B. Infrared and millimetre-wave scintillometry in the suburban environment – part 2: Large-area sensible and latent heat fluxes. *Atmos. Meas. Tech.* **2015**, *8*, 1407–1424. [CrossRef]
19. Bai, J.; Jia, J.; Liu, S.; Xu, Z.; Hu, G.; Zhu, M.; Song, L. Characterizing the footprint of eddy covariance system and large aperture scintillometer measurements to validate satellite-based surface fluxes. *IEEE Geosci. Remote Sens. Lett.* **2015**, *12*, 943–947.
20. Meijninger, W.M.L.; Hartogensis, O.K.; Kousiek, W.; Hoedjes, J.C.B.; Zuurbier, R.M.; Bruin, H.A.R.D. Determination of area-averaged sensible heat fluxes with a large aperture scintillometer over a heterogeneous surface—Flevoland field experiment. *Bound. Layer Meteorol.* **2002**, *105*, 37–62. [CrossRef]
21. Chehbouni, A. Estimation of heat and momentum fluxes over complex terrain using a large aperture scintillometer. *Agric. For. Meteorol.* **2000**, *105*, 215–226. [CrossRef]

22. Beyrich, F.; Bruin, H.A.R.D.; Meijninger, W.L.; Schipper, J.W. Results from one-year continuous operation of a large aperture scintillometer over a heterogeneous land surface. *Bound. Layer Meteorol.* **2001**, *105*, 85–97. [CrossRef]
23. Hemakumara, H.M.; Lalith, C.; Moene, A.F. Evapotranspiration fluxes over mixed vegetations areas measured from large aperture scintillometer. *Agric. Water Manag.* **2003**, *58*, 109–112. [CrossRef]
24. McAneney, K.J.; Green, A.E.; Astill, M.S. Large-aperture scintillometry: The homogeneous case. *Agric. For. Meteorol.* **1995**, *76*, 149–162. [CrossRef]
25. Hoedjes, J.C.B.; Zuurbier, R.M.; Watts, C.J. Large aperture scintillometer used over a homogeneous irrigated area, partly affected by regional advection. *Bound. Layer Meteorol.* **2002**, *105*, 99–117. [CrossRef]
26. Ezzahar, J.; Chehbouni, A.; Er-Raki, S.; Hanich, L. Combining a large aperture scintillometer and estimates of available energy to derive evapotranspiration over several agricultural fields in a semi-arid region. *Plant Biosyst. Int. J. Deal. All Asp. Plant Biol.* **2009**, *143*, 209–221. [CrossRef]
27. Xu, F.; Wang, W.; Wang, J.; Xu, Z.; Qi, Y.; Wu, Y. Area-averaged evapotranspiration over a heterogeneous land surface: Aggregation of multi-point ec flux measurements with high-resolution land-cover map and footprint analysis. *Hydrol. Earth Syst. Sci. Discuss.* **2016**, 1–37. [CrossRef]
28. Liu, S.M.; Xu, Z.W.; Wang, W.Z.; Jia, Z.Z.; Zhu, M.J.; Bai, J.; Wang, J.M. A comparison of eddy-covariance and large aperture scintillometer measurements with respect to the energy balance closure problem. *Hydrol. Earth Syst. Sci. Discuss.* **2011**, *15*, 1291–1306. [CrossRef]
29. Lu, L.; Cheng, Y.; Bian, L.; Lu, C.; Ding, G. A study of the turbulence fluxes transfer of CO_2, sensible heat and latent heat for the surface layer over the typical rice field, yangtdz delta. *Chin. J. Geophys.* **2003**, *46*, 1078–1090. [CrossRef]
30. Timm, A.U.; Roberti, D.R.; Streck, N.A.; Gustavo, G.; de Gonçalves, L.; Acevedo, O.C.; Moraes, O.L.L.; Moreira, V.S.; Degrazia, G.A.; Ferlan, M.; et al. Energy partitioning and evapotranspiration over a rice paddy in southern brazil. *J. Hydrometeorol.* **2014**, *15*, 1975–1988. [CrossRef]
31. Harazono, Y.; Kim, J.; Miyata, A.; Choi, T.; Yun, J.-T.; Kim, J.-W. Measurement of energy budget components during the international rice experiment (irex) in Japan. *Hydrol. Process.* **1998**, *12*, 2081–2092. [CrossRef]
32. Shi, S.; Huang, B.; Liu, S.; Yang, Y.; Huang, Y.; Xu, Z. Development of ameasuring system for surface energy and water vapor fluxes at large scale. *Adv. Atmos. Sci.* **2010**, *25*, 1128–1138.
33. Dyer, A.J. A review of flux-profile relationships. *Bound. Layer Meteorol.* **1974**, *7*, 363–372. [CrossRef]
34. Vickers, D.; Mahrt, L. Quality control and flux sampling problems for tower and aircraft data. *J. Atmos. Ocean. Technol.* **1997**, *14*, 512–526. [CrossRef]
35. Moncrieff, J.; Clement, R.; Finnigan, J.; Meyers, T. Averaging, detrending, and filtering of eddy covariance time series. In *Handbook of Micrometeorology*; Lee, X.H., Massman, W., Law, B., Eds.; Springer: New York, NY, USA, 2004; pp. 7–31.
36. Moncrieff, J.B.; Massheder, J.; De Bruin, H.; Elbers, J.; Friborg, T.; Heusinkveld, B.; Kabat, P.; Scott, S.; Soegaard, H.; Verhoef, A. A system to measure surface fluxes of momentum, sensible heat, water vapour and carbon dioxide. *J. Hydrol.* **1997**, *188*, 589–611. [CrossRef]
37. Burba, G.; Schmidt, A.; Scott, R.L.; Nakai, T.; Kathilankal, J.; Fratini, G.; Hanson, C.; Law, B.; McDermitt, D.K.; Eckles, R. Calculating CO_2 and H_2O eddy covariance fluxes from an enclosed gas analyzer using an instantaneous mixing ratio. *Glob. Chang. Biol.* **2012**, *18*, 385–399. [CrossRef]
38. Wang, T.-I.; Ochs, G.; Clifford, S. A saturation-resistant optical scintillometer to measure C_n^2. *J. Opt. Soc. Am.* **1978**, *68*, 334–338. [CrossRef]
39. Hill, R.; Clifford, S.; Lawrence, R. Refractive-index and absorption fluctuations in the infrared caused by temperature, humidity, and pressure fluctuations. *J. Opt. Soc. Am.* **1980**, *70*, 1192–1205. [CrossRef]
40. Wesely, M.L. The combined effect of temperature and humidity fluctuations on refractive index. *J. Appl. Meteorol.* **1976**, *15*, 43–49. [CrossRef]
41. Odhiambo, G.; Savage, M. Sensible heat flux by surface layer scintillometry and eddy covariance over a mixed grassland community as affected by bowen ratio and most formulations for unstable conditions. *J. Hydrometeorol.* **2009**, *10*, 479–492. [CrossRef]
42. Ochs, G.R.; Hill, R.J. Optical-scintillation method of measuring turbulence inner scale. *Appl. Opt.* **1985**, *24*, 2430–2432. [CrossRef] [PubMed]
43. Wyngaard, J.; Izumi, Y.; Collins, S.A. Behavior of the refractive-index-structure parameter near the ground. *J. Opt. Soc. Am.* **1971**, *61*, 1646–1650. [CrossRef]

44. Wyngaard, J.C. *On Surface Layer Turbulence*; Haugen, D.A., Ed.; Workshop on Micrometeorology; American Meteorological Society: Boston, MA, USA, 1973; pp. 101–149.
45. Andreas, E.L. Estimating Cn2 over snow and sea ice from meteorological data. *J. Opt. Soc. Am.* **1988**, *5*, 481–495. [CrossRef]
46. Thiermann, V.; Grassl, H. The measurement of turbulent surface-layer fluxes by use of bichromatic scintillation. *Bound. Layer Meteorol.* **1992**, *58*, 367–389. [CrossRef]
47. De Bruin, H.; Kohsiek, W.; Van den Hurk, B. A verification of some methods to determine the fluxes of momentum, sensible heat, and water vapour using standard deviation and structure parameter of scalar meteorological quantities. *Bound. Layer Meteorol.* **1993**, *63*, 231–257. [CrossRef]
48. Kaimal, J.C.; Finnigan, J.J. *Atmospheric Boundary Layer Flows: Their Structure and Measurement*; Oxford University Press: New York, NY, USA, 1994.
49. Edson, J.B.; Fairall, C.W. Similarity relationships in the marine atmospheric surface layer for terms in the tke and scalar variance budgets. *J. Atmos. Sci.* **1998**, *55*, 2311–2328. [CrossRef]
50. Gruber, M.; Fochesatto, G.J. A new sensitivity analysis and solution method for scintillometer measurements of area-averaged turbulent fluxes. *Bound. Layer Meteorol.* **2013**, *149*, 65–83. [CrossRef]
51. Finkelstein, P.L.; Sims, P.F. Sampling error in eddy correlation flux measurements. *J. Geophys. Res. Atmos.* **2001**, *106*, 3503–3509. [CrossRef]
52. Gruber, M.A.; Fochesatto, G.J.; Hartogensis, O.K.; Lysy, M. Functional derivatives applied to error propagation of uncertainties in topography to large-aperture scintillometer-derived heat fluxes. *Atmos. Meas. Tech.* **2014**, *7*, 2361–2371. [CrossRef]
53. Hartogensis, O.K.; Watts, C.J.; Rodriguez, J.C.; Bruin, H.A.R.D. Derivation of an effective height for scintillometers la poza experiment in Northwest Mexico. *J. Hydrometeorol.* **2003**, *4*, 915–928. [CrossRef]
54. Peng, G.; Xuhui, C.; Shaomin, L. A flux footprint model for large aperture scintillometer. *Acta Sci. Nat. Univ. Pekin* **2007**, *43*, 822–827.
55. Kormann, R.; Meixner, F.X. An analytical footprint model for non-neutral stratification. *Bound. Layer Meteorol.* **2001**, *99*, 207–224. [CrossRef]
56. Kleissl, J.; Hong, S.-H.; Hendrickx, J.M.H. New mexico scintillometer network: Supporting remote sensing and hydrologic and meteorological models. *Bull. Am. Meteorol. Soc.* **2009**, *90*, 207–218. [CrossRef]
57. Alfieri, J.G.; Blanken, P.D. How representative is a point? The spatial variability of surface energy fluxes across short distances in a sand-sagebrush ecosystem. *J. Arid Environ.* **2012**, *87*, 42–49. [CrossRef]
58. Zhang, H.; Zhang, H.; Cai, X.; Song, Y.; Sun, J. Contribution of low-frequency motions to sensible heat fluxes over urban and suburban areas. *Bound. Layer Meteorol.* **2016**, *161*, 183–201. [CrossRef]